Modeling and experimental strain measurements on a non-homogeneous cylinder under transverse load

John A. Viator[a,b], Stephen Kreger[a], Michele W. Winz[a], and Eric Udd[a]

[a]Blue Road Research, Fairview, OR, USA

[b]Oregon Health & Science University, Portland, OR, USA

ABSTRACT

Optical fiber sensors have the capability of sensing environmental factors, including strain and temperature. In particular, optical fiber Bragg gratings have been used to create multi-parameter sensors capable of measuring axial and transverse strain in addition to temperature. These measurements are made by writing gratings into optical fibers at two separated wavelengths, 1300 and 1550 nm, and monitoring the polarization sensitive output from the sensor. While there is an analytical model for determining the strain on a homogeneous cylinder under transverse load, these fiber optic sensors are not homogeneous as they consist of distinct regions within the fiber: core, cladding, and stress rods. We measure the strain on a multi-parameter fiber Bragg grating written at 1550 nm under transverse load at 0, 15, 30, 45, 60, 75, and 90 ° and compare these values with an analytical solution accounting for internal stresses and transverse load.

Keywords: optical fiber, stress rods, polarization, fiber Bragg grating

1. INTRODUCTION

Fiber optic strain sensors are used for non-destructive sensing in aerospace, civil structures, and other industries [1]. In particular, fiber optic Bragg sensors have been studied for strain and temperature sensing. Using polarization maintaining optical fiber, fiber Bragg gratings (FBGs) may be used to monitor strain in three axes: longitudinally (along the longitudinal axis of the fiber) and in two orthogonal transverse directions of the fiber [2–5]. Many attempts have been undertaken to extract strain information from reflected peaks from FBGs. These attempts have centered around linear methods using algebraic functions relating FBG response to strain in three aforementioned directions and temperature.

In this study, we experimentally determined the response of a FBG under transverse load and compared these results to theoretical strain models of non-homogeneous cylinders. Though the response of a homogeneous cylinder under transverse load can be analytically stated [6], the total stress on a FBG is a combination of the external load and the internal stresses induced by different material regions within the fiber. The different material regions are included in the optical fiber manufacturing process in order to induce birefringence in the core, allowing the fiber to be used as a polarization maintaining (PM) medium. We suggest a model of principal stress on FBG and undertake measurements of transverse load on FBGs written in PM optical fiber. We also analyze the reflected peaks of both polarization states on transverse loaded FBGs in order to observe behavior which may indicate the magnitude of the internal stress on the FBGs.

2. MATERIALS AND METHODS

2.1. Strain measurements

The apparatus for testing the strain on the optical fiber is shown in Figure 1. It consisted of a 1550 nm ASE light source (NP Photonics, Inc., Tucson, AZ) coupled to a 50/50 splitter via PM optical fiber. The FBG was written into PM fiber with bow-tie stress rods. One segment continued to a FBG under transverse load, while

Further author information: (Send correspondence to J.A.V.)

J.A.V.: E-mail: viatorj@ohsu.edu, Telephone: 1 503-667-7772 Address: Blue Road Research, 376 NE 219^{th} Avenue, Grersham, OR 97030

Report Documentation Page

Form Approved
OMB No. 0704-0188

1. REPORT DATE	2. REPORT TYPE	3. DATES COVERED
2004		**00-00-2004 to 00-00-2004**

4. TITLE AND SUBTITLE	5a. CONTRACT NUMBER
Modeling and experimental strain measurements on a non-homogeneous cylinder under traverse load	5b. GRANT NUMBER
	5c. PROGRAM ELEMENT NUMBER
6. AUTHOR(S)	5d. PROJECT NUMBER
	5e. TASK NUMBER
	5f. WORK UNIT NUMBER
7. PERFORMING ORGANIZATION NAME(S) AND ADDRESS(ES) **Blue Road Research,376 NE 219th Avenue,Gresham,OR,97030**	8. PERFORMING ORGANIZATION REPORT NUMBER
9. SPONSORING/MONITORING AGENCY NAME(S) AND ADDRESS(ES)	10. SPONSOR/MONITOR'S ACRONYM(S)
	11. SPONSOR/MONITOR'S REPORT NUMBER(S)

12. DISTRIBUTION/AVAILABILITY STATEMENT
Approved for public release; distribution unlimited

13. SUPPLEMENTARY NOTES

14. ABSTRACT
see report

15. SUBJECT TERMS

16. SECURITY CLASSIFICATION OF:			17. LIMITATION OF ABSTRACT	18. NUMBER OF PAGES	19a. NAME OF RESPONSIBLE PERSON
a. REPORT **unclassified**	b. ABSTRACT **unclassified**	c. THIS PAGE **unclassified**		**7**	

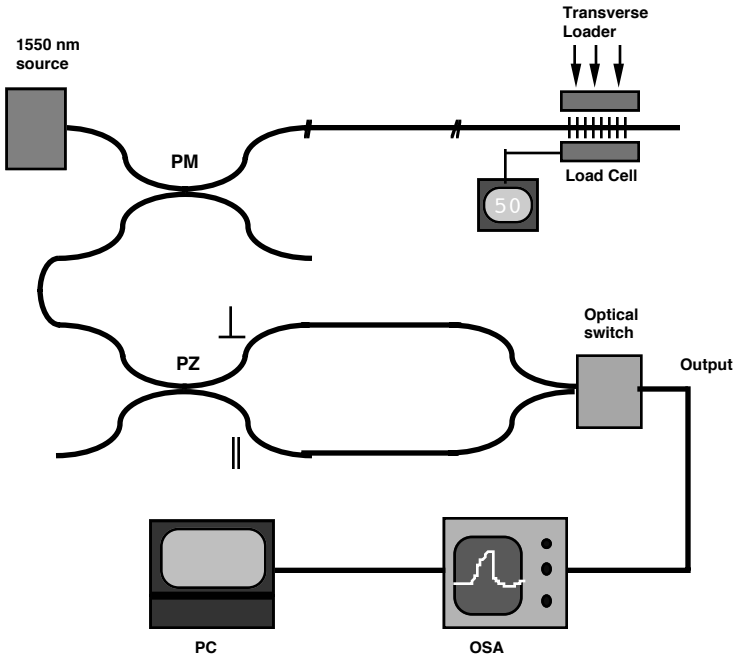

Figure 1. The schematic of the system for measuring transverse load is shown here.

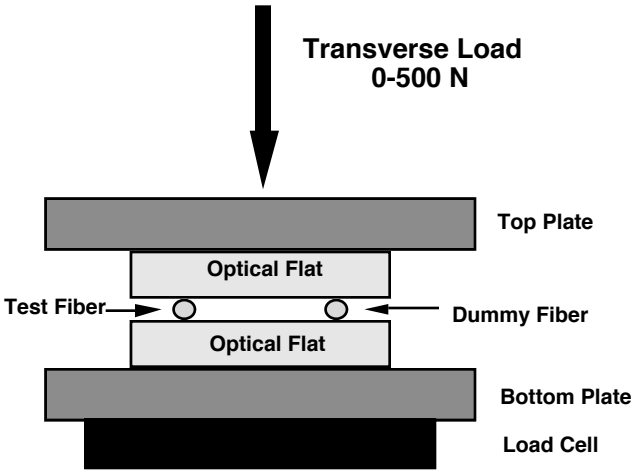

Figure 2. The geometry of the transverse loader is shown here. The dummy fiber is used to ensure the silica plates are parallel.

the other segment was coupled to polarizing (PZ) optical fiber. The PZ fiber was sent through an optical switch that alternated between parallel and perpendicular polarization states in order to select the fast and slow axes reflected from the FBG. The output from the optical switch was sent to an optical spectrum analyzer (AQ6317B, Ando Electric Co., Ltd., Kanagawa, Japan), and the sampled data was stored on a computer. The user interface was developed using LabView (National Instruments, Austin, TX). The user interface stored the waveforms along with the applied force, time of sample, and fast and slow axes peak positions.

The transverse loader set up is shown in Figure 2. It consisted of two stainless steel plates with 1" fused silica optical flats (Esco Products, Oak Ridge, NJ) attached to their opposing faces. The flatness was rated at $\lambda/4$. The FBG was set between the optical flats. A stripped dummy fiber, approximately 10 cm long, was also placed

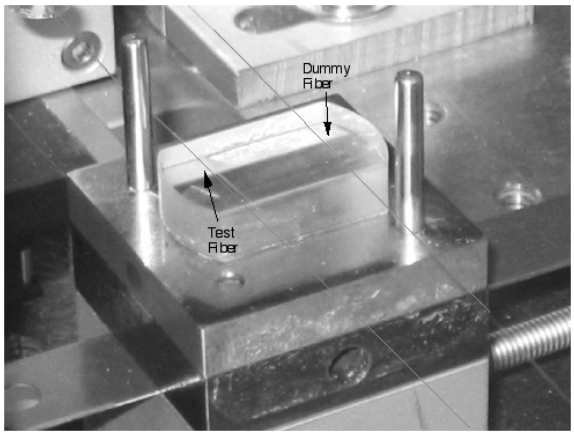

Figure 3. A photograph of the two fibers on the bottom plate of the transverse loader is shown here.

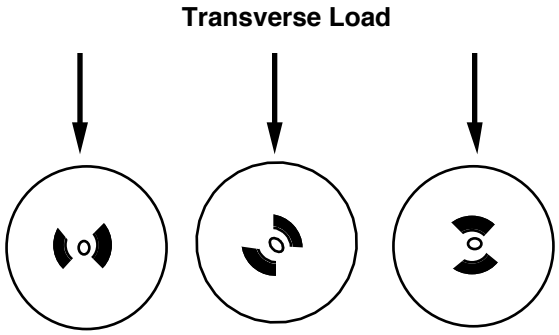

Figure 4. The rotation of the optical fiber causes the orientation of the stress rods to change with respect to the externally applied load.

between the flats in order to ensure even loading of the FBG. The test and dummy fiber were carefully positioned equidistant from the load point to ensure equal loading between the fibers. The width of the optical flats in contact with the fibers was 14.8 mm. The applied force to the transverse loader was 0–700 N, at approximately 50 N increments. The FBG was rotated from 0–90° in 15° increments. A photograph of the fiber on the bottom plate is shown in Figure 3.

The effect of changing the homogeneity of the glass cylinder by rotation of bow tie fiber, used in these experiments, is shown in Figure 4. The optical fiber was composed of fused silica, while the core and bow tie stress rods were fused silica doped with Germanium and Boron, respectively. Internal stresses induced by the rods change orientation with fiber rotation, changing the sum of stresses which includes externally applied transverse load.

2.2. Strain modeling

The shift in wavelength $\Delta\lambda$ of Bragg grating reflection peaks polarized in the x and y directions orthogonal to the fiber axis in response to strain ϵ and temperature T can be expressed as,

$$\frac{\Delta\lambda_x}{\lambda_0} = \left(1 - \frac{\mathrm{n}_0^2}{2}\mathrm{p}_{12}\right)\epsilon_z - \left(\frac{\mathrm{n}_0^2}{2}\mathrm{p}_{11}\right)\epsilon_x - \left(\frac{\mathrm{n}_0^2}{2}\mathrm{p}_{12}\right)\epsilon_y + \left(\frac{1}{\mathrm{n}_0}\frac{d\mathrm{n}_0}{d\mathrm{T}} + \frac{\mathrm{n}_0^2}{2}\left(\mathrm{p}_{11} + 2\mathrm{p}_{12}\right)\alpha\right)\Delta\mathrm{T} \tag{1}$$

$$\frac{\Delta\lambda_y}{\lambda_0} = \left(1 - \frac{\mathrm{n}_0^2}{2}\mathrm{p}_{12}\right)\epsilon_z - \left(\frac{\mathrm{n}_0^2}{2}\mathrm{p}_{12}\right)\epsilon_x - \left(\frac{\mathrm{n}_0^2}{2}\mathrm{p}_{11}\right)\epsilon_y + \left(\frac{1}{\mathrm{n}_0}\frac{d\mathrm{n}_0}{d\mathrm{T}} + \frac{\mathrm{n}_0^2}{2}\left(\mathrm{p}_{11} + 2\mathrm{p}_{12}\right)\alpha\right)\Delta\mathrm{T} \tag{2}$$

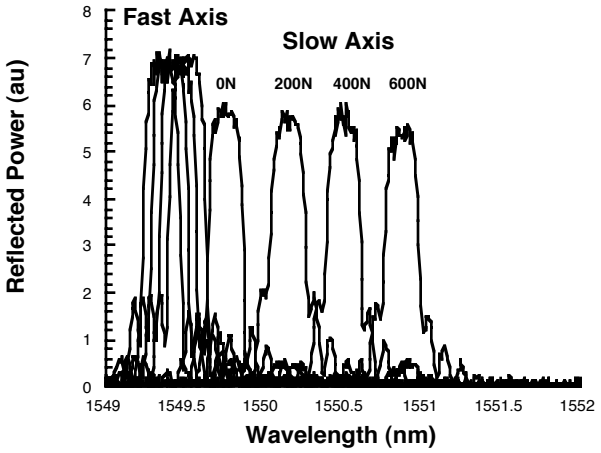

Figure 5. The reflected peaks are shown here for 0, 200, 400, and 600 N. The slow axis is shown clustered at left, while the fast axis peaks are shown more widely separated on the right.

In the above equations, p_{ij} are components of the strain-optic tensor, n_0 is the effective index of the mode propagating in the core, λ_0 is the center wavelength of the grating in the unstrained state, and α is the thermal expansion coefficient. Since the loading apparatus is at thermal equilibrium and has a large thermal mass, we will neglect temperature change during the loading tests. For a typical germanosilicate optical fiber $p_{12} = 0.252$, $p_{11} = 0.113$, $n_0 = 1.46$ [7]. If transverse strain is limited to the x-direction and we assume there are no other forces or constraints on the fiber so that $\epsilon_x = \epsilon_y = -\nu\epsilon_z$, peak separation is a linear function of the transverse strain:

$$\frac{\lambda_x - \lambda_y}{\lambda_0} = \frac{n_0^2}{2}\left(p_{12} - p_{11}\right)\left(1 - \nu\right)\epsilon_x \tag{3}$$

where $\nu = 0.17$ is the Poisson ratio.

In order to model the total load on an optical fiber that experiences internal stresses due to material inhomogeneities along with external forces, we propose the following two equations, which give the prinicipal stresses as,

$$\sigma_{p1} = \frac{1}{2}\left[\sigma_n + \sigma_t + \sigma_x + \sigma_y + \sqrt{(\sigma_n - \sigma_t)^2 + (\sigma_x - \sigma_y)^2 + 2(\sigma_n - \sigma_t)(\sigma_x - \sigma_y)\cos\left(2\beta\right)}\right] \tag{4}$$

$$\sigma_{p2} = \frac{1}{2}\left[\sigma_n + \sigma_t + \sigma_x + \sigma_y - \sqrt{(\sigma_n - \sigma_t)^2 + (\sigma_x - \sigma_y)^2 + 2(\sigma_n - \sigma_t)(\sigma_x - \sigma_y)\cos\left(2\beta\right)}\right] \tag{5}$$

Here, σ_n is the externally applied stress at angle β, σ_t is the external stress at $\beta + 90\,^\circ$, while σ_x and σ_y are the orthogonal internal stresses on the fiber core. We relate σ_n and σ_t by the Poisson ratio, 0.19 [8], making σ_n greater than σ_t by a factor of 5. We modeled this using Mathematica, varying the maximum external load with the internal stress. Specifically we computed the above equations with σ_n and σ_y at various combinations, in order to match the experimental data taken. We show the results for 1:10, 1:3, 1:1, and 3:1.

3. RESULTS

3.1. Reflected Peak Data

The reflected peaks from the FBG loaded at 0, 200, 400, and 600 N is shown in Figure 5. The optical fiber was not rotated in these measurements, making the orientation 0 °. The slow axis peaks are shown clustered around 1549.5 nm while the fast axis peaks are shown centered from 1549.8 nm to 1551 nm.

The ratio of the change in wavelength for the fast and slow axes under load is shown in Figure 6. The data shown as squares is for the fiber at 0 ° orientation, while the data shown as circles is for the fiber at 90 °.

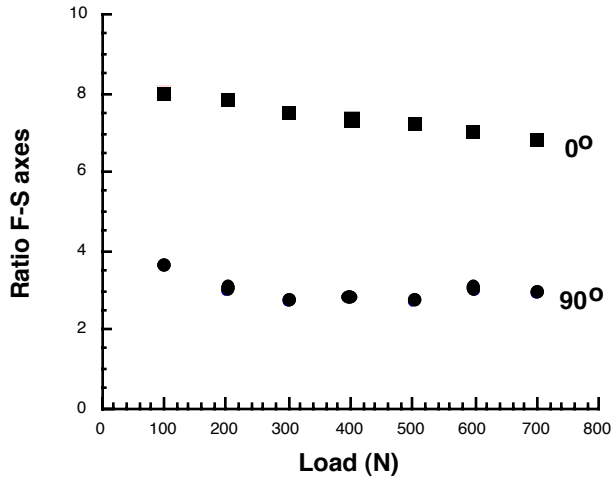

Figure 6. The ratios of the change in wavelength of the fast and slow axes under load are shown for 0 and 90 ° orientation.

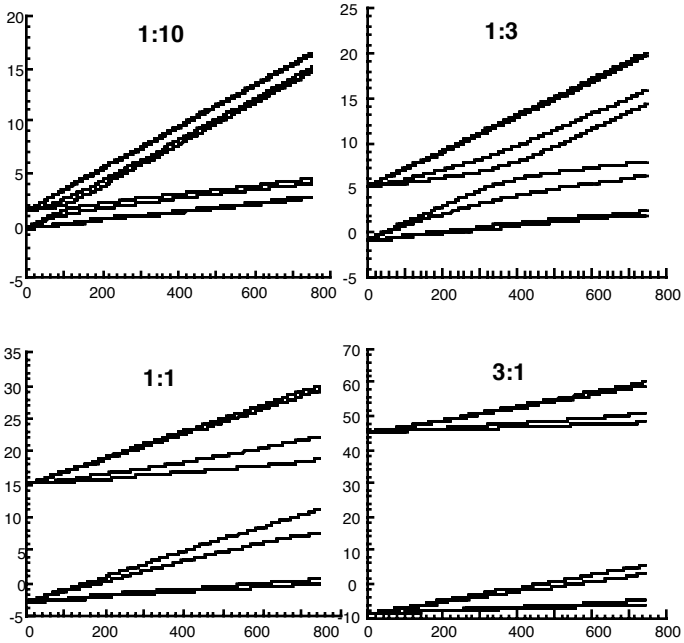

Figure 7. The principal stresses for FBGs according to Equations 4 and 5 are shown here.

3.2. Principal Stress Model

The computed principal stresses for FBGs under load at 0, 30, 60, and 90 ° is shown in Figure 7. Equation **??** was used for these plots. The numbers indicated above each plot are the ratios of the magnitude of the internal stress and the maximum applied load. For example, 1:10 indicates the stress induced internally on the fiber core is 10% of the magnitude of the maximum load on the fiber.

3.3. Experimental Data v. Principal Stress Model

The experimental data is shown with the 1:3 Principal Stress Model in Figure 8.

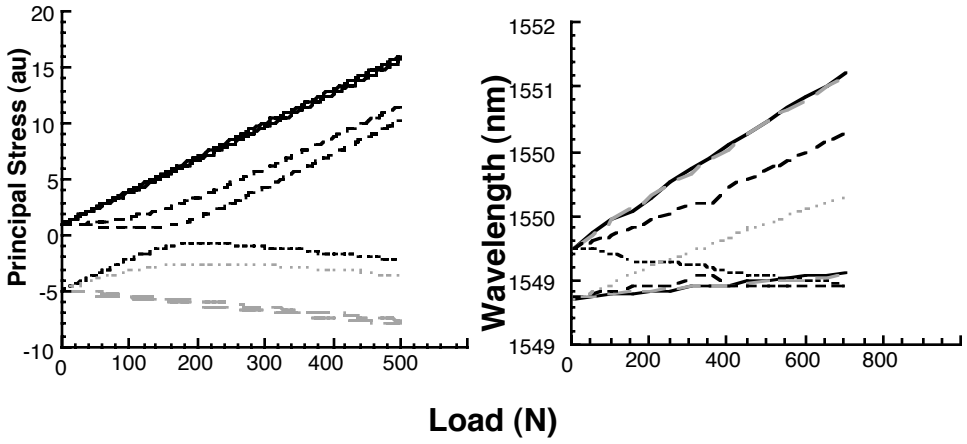

Figure 8. The response of the FBG at various angles is shown along with the principal stress model at 1:3 load ratio.

4. DISCUSSION

Extraction of strain and temperature from analysis of wavelength shifts of reflected peaks from FBGs is a main focus of research on multi-parameter fiber optic sensors. The problem can be written by the system of linear equations,

$$\lambda = \mathbf{K}\delta \tag{6}$$

where λ is a 4X1 vector of wavelength shifts of fast and slow axis components for two wavelengths, such as 1300 nm and 1550 nm. $\mathbf{K}$ is a 4X4 matrix of 4 coefficients (three directions of strain and temperature) for the wavelengths, and δ is a 4X1 vector of strain and temperature.

This paper attempted to better understand the response of FBGs to externally applied transverse loads, taking into account the internal stress used to induce birefringence in PM optical fibers.

4.1. Reflected Peak Data

The data shown in Figure 5 shows how the reflected peaks from the FBG change wavelength in response to external load. For a homogeneous cylinder, the ratio of the fast and slow axes responses at 0 ° (and conversely, the ratio of the slow and fast axes at 90 °) should give the negative reciprocal of the Poisson ratio, as the applied stress would induce a negative stress at a right angle. These stresses would manifest themselves as wavelength shifts in the FBG peaks in a linear manner.

The measured ratios at 0 ° and 90 ° are approximately 7.5 and 3, respectively. Note that the reciprocal of the Poisson ratio, approximately 5.0, resides between these two values. The departure of the ratios from that predicted by the Poisson ratio is certainly due to the internal stresses on the fiber core. At 0 °, the external load and the primary internal stress are aligned, while at 90 ° they are in opposition. Analyzing the ratios at intermediate angles may allow determination of the internal stresses due to the stress rods, giving better understanding of FBG responses to transverse load.

4.2. Principal Stress Model

The principal stress model attempted to reconcile the internal stresses with external load to give a picture of the total stress on the FBG. We modeled several sets of stress parameters, primarily to determine the behavior of reflectance peak changes at different angles for simulated FBGs of various internal stresses. The difference between the Equations 4 and 5 is that the radical term is added in the former and subtracted in the latter. Thus, the fast and slow axes, represented by Equations 4 and 5, respectively, cannot cross. Inspection of the actual data shows crossing of the fast and slow axes for the 90 ° data, however. This phenomenon is addressed next.

4.3. Experimental Data v. Principal Stress Model

While the principal stress model for load ratio 1:3 most closely resembles the actual measured data shown in Figure 8, some differences exist that should be addressed. The nonlinearity evident in the model at about 170 N does not exist in the experimental data. More obviously, however, is that the experimental data shows a crossing in the 90 ° lines, while the model does not permit this.

4.4. Future Work

Further data will be taken in order to improve the representative curves for the FBGs under load at various angles. Improving the quality of the curves may reveal the expected nonlinearities. Additionally, increasing the load to greater than 700 N may show the region of nonlinearity. Also, improved analysis for identifying peaks could improve the quality of the curves. We will also develop methods for possibly extracting the actual internal stresses from the ratio of the fast and slow axes responses, as shown in Figure 6. This additional work may eventually allow solution of Equation 6 or at least guide the approximation of strain determination from FBG peak responses.

We will continue modeling studies using finite element analysis to simulate bow-tie stress rods with the appropriate material properties. This analysis will give us a better understanding of the effective Poisson ratio, which is negative, as seen in Figure 8. Using this result, we should be able to test the range of validity in the 4X4 matrix method calculation. Additionally, we will do experiments in which we vary temperature, validating the theoretical model and investigating the temperature dependence of Poisson's ratio.

ACKNOWLEDGMENTS

The authors would like to acknowledge Marley Kunzler, Wesley Kunzler, and Tad Taylor of Blue Road Research for their assistance with the experiments in this paper. We acknowledge support of the Air Force Research Laboratory contract F33615-02-C-5043.

REFERENCES

1. E. Udd, *Fiber Optic Smart Structures*, Wiley-Interscience, Hoboken, NJ, 1995.
2. C. M. Lawrence, D. V. Nelson, and E. Udd, "Multi-parameter sensing with fiber bragg gratings," in *Second Pacific Northwest Fiber Optic Sensor Workshop*, E. Udd, ed., *Proc. SPIE* **2872**, pp. 24–31, 1996.
3. C. M. Lawrence, D. V. Nelson, E. A. Fuchs, J. R. Spingarn, and T. E. Bennet, "Fiber optic sensors at sandia national laboratories," in *Second Pacific Northwest Fiber Optic Sensor Workshop*, E. Udd, ed., *Proc. SPIE* **2872**, pp. 72–78, 1996.
4. C. M. Lawrence, D. V. Nelson, A. Makino, and E. Udd, "Modeling of the multi-parameter bragg grating sensor," in *Third Pacific Northwest Fiber Optic Sensor Workshop*, E. Udd and C. C. Jung, eds., *Proc. SPIE* **3180**, pp. 42–49, 1997.
5. C. M. Lawrence, D. V. Nelson, T. E. Bennet, and J. R. Spingarn, "An embedded fiber optic sensor method for determining residual stresses in fiber reinforced composite materials," *J. Intell. Mater. Syst. Struc.* **9**, pp. 788–799, 1999.
6. S. Timoshenko, *Theory of Elasticity*, McGraw-Hill, New York, NY, 1970.
7. A. Orthonos and K. Kalli, *Fiber Bragg Gratings: fundamentals and applications in telecommunications and sensing*, Artech House, Norwood, MA, 1999.
8. R. B. Wagreich, W. A. Atia, H. Singh, and J. S. Sirkis, "Effects of diametric load on fibre bragg gratings fabricated in low birefringent fiber," *Electron. Lett.* **32**, pp. 1223–1224, 1996.